RSC Advances

PAPER

View Article Online
View Journal | View Issue

Cite this: *RSC Adv.*, 2026, **16**, 20169

pH-responsive Ni-MOF based nanocarriers with folic acid targeting for enhanced chemotherapeutic efficacy in breast cancer

Komal Zaman Khan,[a] Ammar Saleem,[a] Eman Fayad,[b] Aurang Zaib,[a] Ghazanfar Abbas,[a] Dalal Nasser Binjawhar,[c] Ali Junaid,[d] Muhammad Naeem Ashiq,[d] Zahid Shafiq *[d] and Hua-Li Qin *[a]

Breast cancer is among the most prevalent malignancies affecting women globally. Conventional chemotherapeutic treatments like 5-fluorouracil (5-FU) are not very effective and can cause serious side effects. To address these challenges, we developed a folic acid-functionalized nickel-based metal–organic framework incorporated with 5-fluorouracil (FA/Ni-MOF/5-FU) as a targeted and pH-responsive nanocarrier for selective breast cancer treatment. The addition of folic acid (FA) made it possible to actively target folate receptors, which are found in high amounts on MDA-MB-231 breast cancer cells. The Ni-MOF acted as biocompatible carrier for controlled drug release. *In vitro* cytotoxicity assays demonstrated that FA/Ni-MOF/5-FU exhibited superior anticancer efficacy against MDA-MB-231 cells, achieving 83.51% inhibition at 40 μM with IC_{50} value of 18.5 ± 0.4 μM, compared with free 5-FU (71.23% inhibition, IC_{50} = 24.4 ± 0.6 μM) and Ni-MOF/5-FU (75.32% inhibition, IC_{50} = 23.6 ± 0.4 μM). FA/Ni-MOF/5-FU had much less cytotoxicity towards normal MCF-10A breast epithelial cells, keeping 86.54% of them alive (IC_{50} > 40 μM). Free 5-FU was more toxic (78.43% of them alive, IC_{50} > 40 μM). The uncoated Ni-MOF had very little effect on both cancer and normal cells (58.91% inhibition on MDA-MB-231 and 13.63% on MCF-10A, IC_{50} > 40 μM), which shows that it is naturally biocompatible. FA/Ni-MOF/5-FU is a promising nanoplatform for targeted breast cancer chemotherapy. It has better tumor selectivity, folate receptor-mediated uptake, and less systemic toxicity than free 5-FU.

Received 21st January 2026
Accepted 18th March 2026

DOI: 10.1039/d6ra00551a

rsc.li/rsc-advances

1 Introduction

Cancer is one of the most serious health problems in the world. In 2018, about 17 million new cancer cases were diagnosed worldwide.[1,2] By 2040, this is projected to rise to around 27.5 million annually due to population growth, aging, and changing risk factors.[3] Breast cancer is currently the most prevalent type of cancer among women, accounting for around 25% of all cancer cases worldwide.[4] It affects women more than any other cancer, and it is also the deadliest.[2] Every year, almost one million new cases are identified.[5] Chemotherapy remains a vital component of cancer therapy, even though surgery, radiotherapy, hormone therapy, and immunomodulation have all improved.[6] However, standard chemotherapy has a problem with drugs spreading throughout the body in a way that isn't specific, which means that the therapeutic dose doesn't reach cancer cells and normal tissues and organs are harmed.[7] This lack of specificity can cause serious side effects like fatigue, nausea, liver damage, and bone marrow suppression, which can be dangerous for the patient.[8] Chemotherapy treatments differ in cost, malignancies, obscure attributes, and adverse effects. These complexities are addressed by identifying alternate therapy or medications.[9]

Scientists are developing advanced drug delivery systems (DDS) selectively transport anticancer drugs directly breast tumor sites, aiming to minimize systemic toxicity, improve pharmacokinetics, enhance bioavailability, increase drug solubility, overcome multidrug resistance, and deliver more active, safer, and personalized therapies with significantly less side effects.[10] Nanotechnology, especially metal–organic frameworks (MOFs), is a basic technology for developing efficient drug delivery systems.[11] MOFs are a relatively recent nanomaterial, and offer exceptional advantages as pharmaceutical nanocarriers due to their higher biocompatibility, higher surface area and porosity for superior drug loading, and remarkable structural flexibility that allows precise tuning of both the framework and its internal pores for optimized encapsulation,

[a]*School of Chemistry, Chemical Engineering and Life Sciences, Wuhan University of Technology, Wuhan 430070, China. E-mail: qinhuali@whut.edu.cn*
[b]*Department of Biotechnology, College of Science, Taif University, P.O. Box 11099, Taif 21944, Saudi Arabia*
[c]*Department of Chemistry, College of Science, Princess Nourah Bint Abdulrahman University, P.O. Box 84428, Riyadh 11671, Saudi Arabia*
[d]*Institute of Chemical Sciences, Bahauddin Zakariya University, Multan-60800, Pakistan. E-mail: zahidshafiq@bzu.edu.pk*

stability, and controlled release.[12] Organic ligands serve as multifunctional linkers, coordinating with metal ions or clusters to form highly ordered, crystalline porous structures ideal for hosting and transporting therapeutic agents.[13] Nickel-based MOFs (Ni-MOFs) have developed as particularly capable candidates in biomedical research, coordination chemistry of Ni(II) ions to create biocompatible, stable, and porous frameworks that can be engineered with diverse organic linkers to exhibit pH-sensitive behavior remaining intact under physiological conditions while undergoing controlled degradation or structural change in the acidic tumor microenvironment (pH 5.0).[14] Ni-MOF offers distinct advantages over other metal-based MOFs like Zn-, Fe-, and Zr-based systems, including superior biocompatibility, high drug loading efficiency and pH-responsive release in the acidic tumor microenvironment. These features, along with its cost-effectiveness and simpler synthesis, make Ni-MOF a promising candidate for targeted breast cancer therapy. This pH-responsiveness enables two key benefits for anticancer therapy: targeted and controlled drug release at tumor sites with minimal premature leakage in healthy tissues, and enhanced therapeutic efficacy through improved drug accumulation, reduced off-target toxicity, and markedly reduced off-target toxicity too standard treatments.[15]

5-Fluorouracil (5-FU) has been used many years a chemotherapy agent for many types of solid tumors. These include breast cancer, colon cancer and liver cancer.[16] 5-FU is a pyrimidine analogue that largely inhibits thymidylate synthase, blocking DNA and RNA synthesis and inducing apoptosis in rapidly dividing cancer cells.[17] 5-FU is wide-spread in clinical practice, the limitations of this drug also exist (*e.g.*, poor solubility, rapid degradation, short plasma half-life, as well as lack of selectivity for tumors), resulting in the necessity to administer 5-FU at high doses to achieve therapeutic levels and associated increased incidence of systemic toxicity.[18] Therefore, it is possible to overcome many of the obstacles faced with 5-FU by using MOF nanocarriers to encapsulate the drug. This would allow for the controlled, localized and sustained release of 5-FU at the tumor site, thus improving the efficacy of treatment and reducing the risk of side effects associated with the administration of high doses of 5-FU.[19] To increase tumor selectivity of the delivered, MOFs are modified by attaching biocompatible (human-friendly) targeting ligands such as folic acid (FA) that bind strongly to folate receptors (FRs).[20] This receptor-mediated endocytosis would allow for selective uptake of FA-functionalized nanocarriers, enhancing drug delivery and therapeutic efficacy at the tumor location.[21] Drug delivery system, comprised of Ni-MOF for the core structure along with 5-fluorouracil (5-FU), has properties are a stable, biocompatible core structure with high surface area and functionalization of the core structure with FA to enable targeting specific cells and pH sensitivity of the Ni-MOF enabling time-dependent control of drug release in acidic tumor microenvironments, therefore enhancing bioavailability and reducing systemic toxicity associated with 5-FU.[22] The FA-Ni-MOF-5-FU drug-delivery system ultimately enhances treatment efficacy *via* targeted and pH-sensitive release of 5-FU, limiting systemic toxicity and enhancing the pharmacokinetic properties of 5-FU. P. Raju *et al.* synthesized a FU@Eu-MOF nanocomposite with 22.15 wt% loading capacity and drug release was limited to 15.4% at (pH = 7.4) but increased to 53.6% (pH = 6) and 85.3% (pH = 5).[23] J.-J. Shen *et al.* developed a (Luteolin + Matrine) NH_2-MIL-101(Fe) @GO system with 9.8% and 14.1% drug loading efficiencies, showing pH-sensitive release: 54.8% and 60.8% at 5 pH, and 17.8% and 58.3% at pH 7.4, respectively.[24] Yang *et al.* designed a MIL-100@Apa@MPN having drug-loading and encapsulation efficiency of 28.33% and 85.01% respectively, whereas drug release was limited to 42.31% at 7.4 pH increased to 73.72% at acidic pH 5.[25] A. Ahmed *et al.* designed a PEG-FA-NH_2-Fe-BDC for doxorubicin delivery with 97% encapsulation efficiency and 14.5 wt% encapsulation capacity while the pH/US dual responsive DOX release efficiency was 44.4% at pH = 7.4 increasing to 90% at pH = 5.3 with US, while 36% at pH = 7.4 increasing to 70.2% at pH = 5.3 without US.[26]

In this study, a folic acid-functionalized nickel-based metal–organic framework (FA/Ni-MOF) was developed as a targeted nanocarrier, successfully loaded with the anticancer drug 5-fluorouracil (5-FU) for enhanced breast cancer therapy. This medicine is highly targeted towards tumors because the FA ligand attaches to folate receptors, which are overexpressed in MDA-MB-231 breast cancer cells. In the acidic tumor environment, the biocompatible and porous Ni-MOF core facilitates maximum drug loading and pH-responsive release. The FA/Ni-MOF/5-FU system stands out due to its superior drug loading efficiency (81.2%) and pH-responsive drug release, ensuring targeted and controlled release in the acidic tumor microenvironment. The problems with non-specific toxicity and poor pharmacokinetics in conventional 5-FU therapy are effectively addressed by the FA/Ni-MOF/5-FU system, which allows for controlled and receptor-mediated drug administration. The results were shown to have a higher inhibitory effect on cancer cells (83.51% inhibition, IC50: 18.5 ± 0.4 μM) compared to normal MCF-10A cells (86.54% viability, IC_{50} > 40 μM), according to the cytotoxicity study. On the other hand, free 5-FU was more effective against normal MCF-10A cells (78.43% viability, IC50 > 40 μM) and less effective against cancer cells (71.23% inhibition, IC50: 24.4 ± 0.6 μM). The functionalization of FA significantly enhances the efficacy and selectivity of drug delivery based on Ni-MOFs in the treatment of breast cancer.

2 Experimental section

2.1 Materials and methods

We purchased sulfonic acid (RSO_3H, 98%, Sigma Aldrich), Absolute ethanol (C_2H_5OH, 99.9% purity, Sigma Aldrich), *N*,*N*-dimethylformamide (DMF) (C_3H_7NO, 99.8% purity, Sigma Aldrich), Nickel chloride hexahydrate ($NiCl_2 \cdot 6H_2O$ 99%, Sigma Aldrich), 2-isopropylaniline ($C_9H_{13}N$, 99%) 1-(3-dimethylaminopropyl)-3-ethylcarbodiimide hydrochloride (EDC) ($C_8H_{17}N_3$ HCl, 98% purity, Sigma Aldrich), Phosphate buffered saline (bio world, pH 7.4 and 5.0) and Deionized water (H_2O) are also used, with the water being lab-prepared. No further purification was performed on any of these compounds before their use.

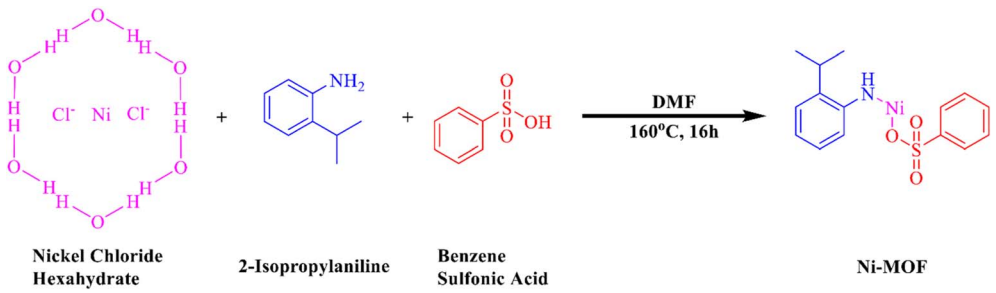

Scheme 1 Reaction scheme of Ni-MOF.

2.2 Characterization

A Rigaku Ultima IV (Japan) diffractometer was used to perform powder X-ray diffraction (PXRD) examination on the synthesised Ni-MOF and its composites. The study used Cu Kα radiation ($\lambda = 1.5406$ Å) across a 2θ range of 10–70°. We used a Nicolet-6700 spectrometer to capture the Fourier-transform infrared (FTIR) spectra in the region of 500–4000 cm^{-1}. We were able to identify the functional groups and verify the successful coordination and drug loading of the nanoparticles through this technique. A German Zeiss (ULTRA 55) scanning electron microscope (SEM) and energy dispersive X-ray spectroscopy (EDX) were used to analyze the surface morphological structure and its elemental composition, while a USA-Thermo Fisher-Tecnai G2 F20 transmission electron microscope (TEM) was used to capture detailed structural images. We used X-ray photoelectron spectroscopy (XPS) on a USA-Thermo Fisher K-Alpha equipment to look at the surface chemical composition and oxidation states. A Malvern Panalytical-Zetasizer Pro (UK) was used to assess the hydrodynamic particle size and zeta potential at room temperature in an aqueous dispersion. Finally, we used a Shimadzu UV-1800 spectrophotometer to do UV-visible spectrophotometric tests to see how well the medicine 5-FU loaded and released.

2.3 Fabrication of Ni-MOF

The Ni-based MOF was created by a hydrothermal process in an autoclave lined with Teflon. After dissolving 20 mmol of nickel chloride hexahydrate in 60 mL of DMF, 20 mmol of 2-isopropylaniline and 10 mmol of sulfonic acid were added. After homogenization, the solution was heated in an autoclave at 160 °C for 16 hours. Precipitate was cooled to room temperature, then centrifuged to separate it. To eliminate any unreacted residues, it was washed three times with DMF. Finally, it dried at 70 °C to get Ni-MOF as shown in Scheme 1.

2.4 Fabrication of Ni-MOF/5-FU

To load 5-fluorouracil (5-FU) into the Ni-based MOF, 0.1 g of the MOF and 0.1 g of 5-FU were mixed in 20 mL of deionized water and sonicated for 30 minutes to make sure they were evenly mixed. Afterwards, the mixture was put for 48 hours in a sealed Teflon container in order to facilitate the inclusion into the mixture of the compound being created. At the end of this process, the solution was separated into its components using centrifugation and the solvent evaporated off by drying under ambient conditions as shown in Scheme 2. Measured the difference between the initial drug concentration and the residual concentration in the supernatant. This was then divided by the total weight of the loaded drug.

The following equation is used to determine the loading efficiency of the drug:

$$\text{Encapsulation efficiency}(\%) = \frac{\text{Mass of incapsulated drug}}{\text{Mass of total drug added}} \times 100$$

In which C_{en} and C_{in} represent the amount of encapsulated 5-FU over its input quantity during the process (mg).

2.5 Folic acid functionalization Ni-MOF

First, 25 mg of folic acid was dissolved in 25 mL of dimethyl sulfoxide (DMSO) using sonication to ensure thorough mixing to make the Ni-MOF functional. The next step was to activate

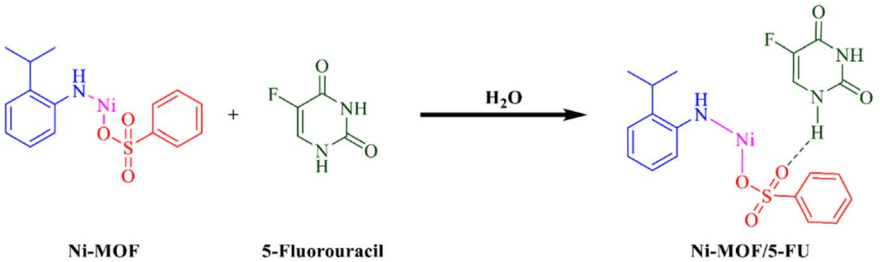

Scheme 2 Reaction scheme of Ni-MOF/5-FU.

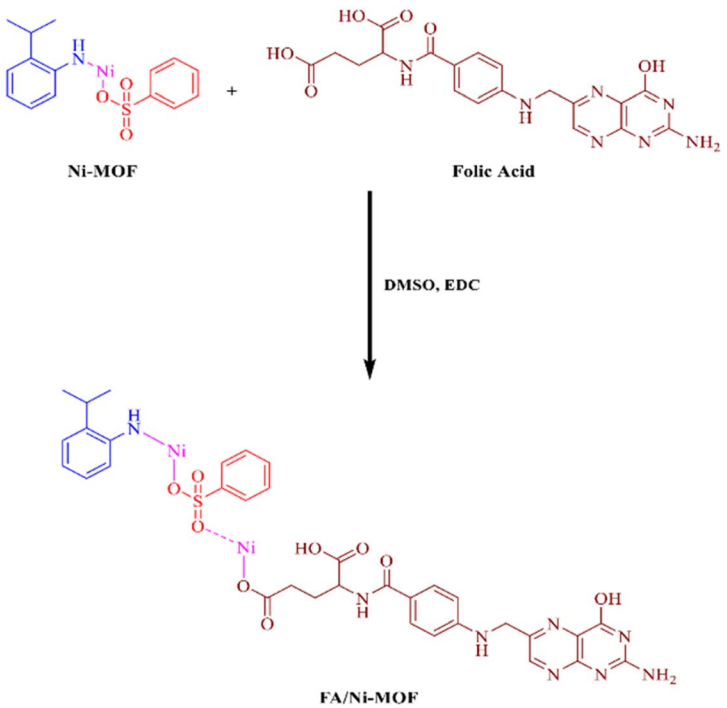

Scheme 3 Reaction scheme of FA/Ni-MOF.

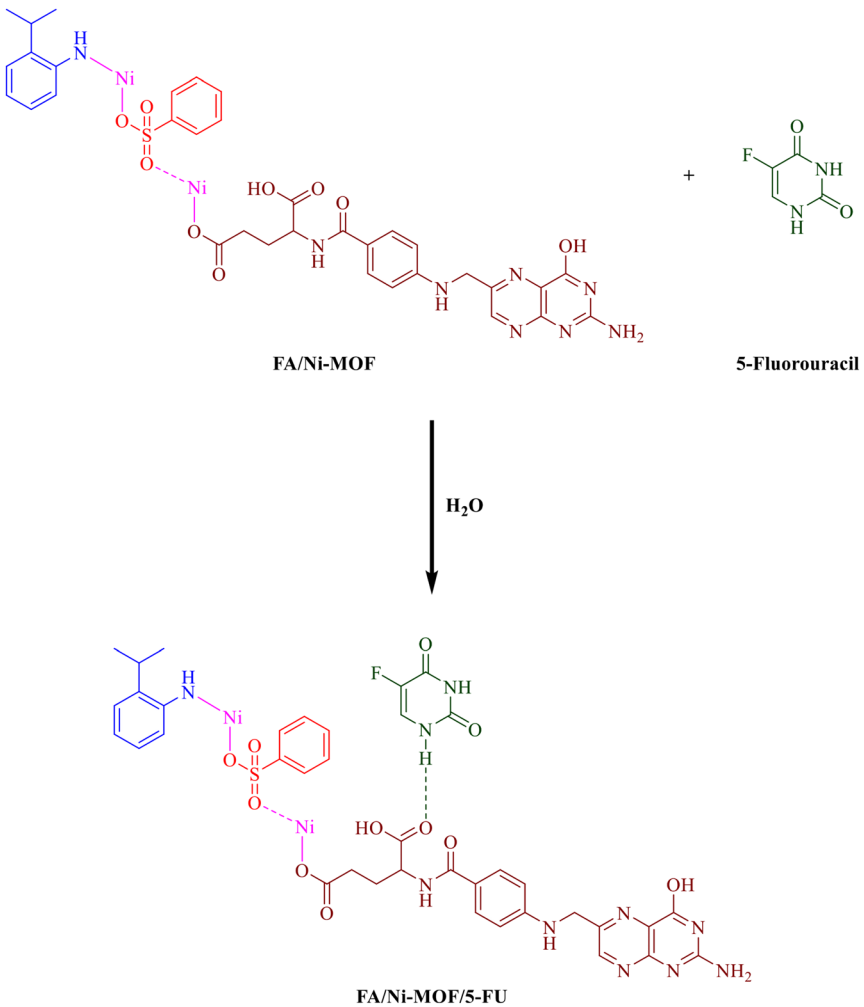

Scheme 4 Reaction scheme of FA/Ni-MOF/5-FU.

the carboxyl groups of folic acid by adding 12 mg of 1-ethyl-3-(3-dimethylaminopropyl) carbodiimide (EDC) and stirring the mixture for 24 hours in the dark. Then, 50 mg of Ni-MOF was added to the reaction mixture in a continuous stirring while pyridine was used to maintain the pH to around 8. Overnight, in darkness, the mixture stirred. Then, it was washed twice with DMSO and six times with deionized water to get unreacted residues. The substance was dried to make the folic acid-functionalized Ni-MOF (FA/Ni-MOF) as shown in Scheme 3.

2.6 Drug loaded FA/Ni-MOF

The procedure for incorporating 5-fluorouracil (5-FU) into the folic acid-modified nickel metal–organic framework (FA/Ni-MOF) consists of combining equal weights (0.1 g each) of both materials into 20 mL of deionized H_2O and subjecting them to sonication for 30 min to achieve completeness of mixing. To facilitate diffusion of the drug throughout the MOF, the resulting mixture was allowed to airtight Teflon container for a period of 36–48 h at ambient temperature with stirring followed by removal of the solution *via* centrifugation; the materials was dry naturally forming 5-FU loaded on FA/Ni-MOF as shown in Scheme 4 and synthesis scheme is given in Scheme 5.

2.7 Synthesis scheme

2.8 Drug delivery

Before the drugs were put inside the Ni-MOF nanocarriers, they were heated in a vacuum at 100 °C for 24 hours to get any enduring solvents and moisture from the pores. To load 5-fluorouracil (5-FU), 100 mg of Ni-MOF was mixed with 30 mL of a 5-FU solution (1000 ppm) and put on an orbital shaker at room temperature for 48 hours. Using a centrifuge, we collected the FA-functionalized 5-FU-loaded Ni-MOF (FA/Ni-MOF/5-FU), washed it multiple times with deionized water, and dried it under vacuum. We used the calibration curve of 5-FU in deionized water ($\lambda_{max} = 266$ nm) to get the drug loading capacity (DLC) and drug loading efficiency (DLE) and then used the following equations.[27] The folic acid-loaded Ni MOF nanoparticles were stored at 4 °C in a dark, dry environment to prevent degradation from light and moisture. During the development process, the nanoparticles were transferred into airtight containers to maintain stability. After synthesis and drug loading, the final product was sealed in sterile vials under inert gas conditions to further protect it from oxidation and moisture. The packaging was designed to preserve the structural integrity and drug release profile, ensuring the system's suitability for targeted cancer therapy.

$$\mathrm{DLE(wt\%)} = \frac{\text{weight of loaded 5 FU}}{\text{intial weight of 5 FU}} \times 100 \quad (1)$$

$$\mathrm{DLC(wt\%)} = \frac{\text{Amount of drug loaded 5 FU(mg)}}{\text{Total weight of carrier(mg)}} \times 100 \quad (2)$$

2.9 Drug release

The pH-responsive release of 5-FU from the FA/Ni-MOF/5-FU nanocarrier was evaluated under tumor microenvironment (pH 5) and physiological (pH 7.4) conditions using phosphate-buffered saline (PBS). In brief, dialysis membrane (3.5 kDa MWCO) holding a tiny quantity of PBS was submerged in 60 mL of PBS buffer at the required pH with 60 mg of FA/Ni-MOF/5-FU. Stirring was used to keep the system at 37 °C. At regular intervals, 1 mL of the release medium was removed and replaced

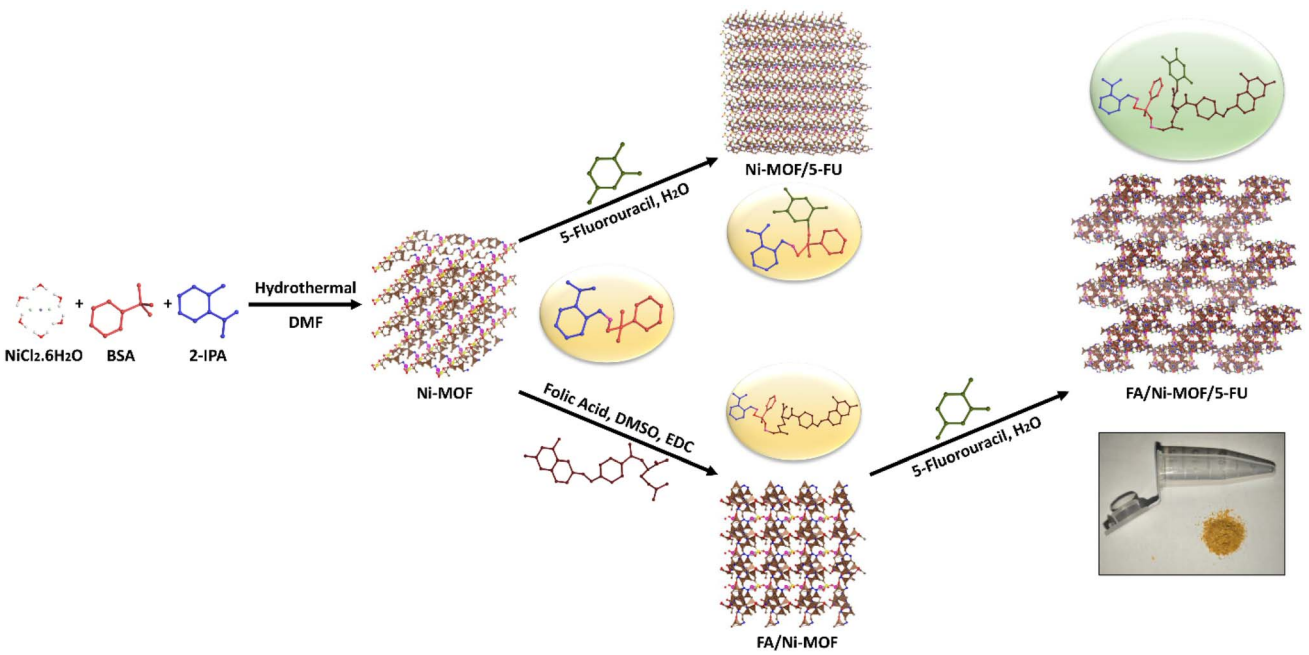

Scheme 5 Synthesis scheme of Ni-MOF, Ni-MOF/5-FU, FA/Ni-MOF, FA/Ni-MOF/5-FU.

with an equivalent amount of fresh PBS to keep the sink conditions constant. A Shimadzu UV-1800 spectrophotometer was used to measure the drug concentration that was released. The measurement was taken at 266 nm. The cumulative release (%) was then determined using the following equation:[28]

$$\text{Drug release(cumulative\%)} = \frac{R_t}{R_f} \times 100 \quad (3)$$

where R_t is the amount of 5-FU released at time t and R_f is the total amount of 5-FU loaded in the FA/Ni-MOF nanocarriers.

2.10 Cell culture

The MCF-10A normal breast epithelial cells and MDA-MB-231 human breast cancer cell line were obtained from the Cell Bank of the Chinese Academy of Sciences (Shanghai, China) and cultured in RPMI-1640 medium supplemented with 10% fetal bovine serum, 1% penicillin-streptomycin, and 2 mM L-glutamine at 37 °C in a humidified atmosphere containing 5% CO_2.

2.11 Cell cytotoxicity assay

The MTT test was used to evaluate the *in vitro* cytotoxicity of 5-FU, Ni-MOF, Ni-MOF/5-FU, FA/Ni-MOF, and FA/Ni-MOF/5-FU. In 96-well plates, MDA-MB-231 and MCF-10A cells were placed at a density of 1×10^1 cells/well and left to incubate for 24 hours. Following that, new medium was added with different concentrations of the test samples (7.81–500 μM) and the mixture was cultured for 48 hours. Each well was then treated with 10 μL of MTT reagent (12 mM) and left to incubate for 4 hours. Following the removal of the medium, 100 μL of DMSO was introduced in order to dissolve the formazan crystals. The PerkinElmer Enspire 2300 multimode plate reader was used to measure the absorbance at 570 nm. A nonlinear regression model in GraphPad Prism 8 was used to generate IC_{50} values, and all tests were performed in triplicate.

2.12 Statistical analysis

The GraphPad Prism 8.0 statistical package was used for all the analysis. The mean ± standard deviation (SD) is used to display the data. We used Kruskal–Wallis test and Dunn's multiple comparison post hoc analysis to see if there was a statistically significant difference between the groups. At $p < 0.05$, differences were deemed to be statistically significant. The significant levels were signified as ****$p \leq 0.0001$, ***$p \leq 0.001$, **$p \leq 0.01$, and *$p \leq 0.05$.

3 Results and discussion

The X-ray diffraction (XRD) analysis successful synthesis and high phase purity of the prepared catalysts. As illustrated in Fig. 1a, the Ni-MOF exhibits distinct diffraction peaks at 2θ values of 11.29°, 13.4°, 14.01°, 14.81°, 15.52°, 16.61°, 17.63°, 19.42°, 22.32°, 24.52°, 26.54°, 27.51°, 29.72°, 33.63°, 43.54°, and 45.32°, reflecting a well-ordered crystalline framework. The addition of 5-Fluorouracil (5-FU) results in a loss of intensity for some of the diffracted peaks in the spectra, indicating that the drug has been successfully encapsulated within the metal–organic framework (MOF). The majority of the diffraction peaks observed for bulk Ni-MOF remain unchanged in their position and relative intensity after the addition of 5-FU, suggesting that the primary crystalline structure of the MOF is preserved. When folic acid (FA) is added to the MOF, new diffraction peaks appear in the X-ray diffractogram at $2\theta = 9.7°$,15.3°,22.8°,28.4°, and 33.9°, indicating that the FA was successfully integrated throughout the Ni-MOF lattice. Furthermore, after the incorporation of FA into the Ni-MOF/5-FU composite, the composite exhibits unique diffraction peaks $2\theta = 9.8°$,15.4°,22.9°,28.53°, and 34.1°, which are slightly shifted from their respective positions prior to addition of FA, thus indicating the presence of structural changes in the MOFs lattice while maintaining phase purity of the remaining constituents. The reduction in peak intensity and positional shift suggests a strong interaction between FA, 5-FU, and the Ni-MOF. Based on the average values of crystallite size calculated from the Debye–Sherrer equation, it was found that the average sizes were 71.35 nm for Ni-MOF and decreased to 53.21 nm with the addition of 5-FU and finally to 37.42 nm upon the incorporation of FA. This indicates that the incorporation of FA and drug encapsulation were effective in reducing the size of the MOF particles and that the size reduction enhances the compactness and stability of the material.

$$D = K\lambda/\beta \cos\theta \quad (4)$$

The value of β is defined as the full width at half maximum (FWHA) for each diffraction peak where θ is the angle of diffraction and λ is the X-ray wavelength. The addition of 5-FU and FA alters the porosity and crystallinity of the Ni-MOF, resulting in slower, more controlled drug release. These modifications decrease crystallinity, enhance drug delivery and gradual diffusion. The loss of peak intensity and slight shifts in diffraction peaks confirm these structural changes.[29]

Ethanol is used as a solvent to react with folic acid (FA) form a stable complex of FA and nickel metal–organic framework (MOF). The FA/Ni-MOF complex has the ability to bind to the chemotherapy drug 5-fluorouracil (5-FU), which results in multifunctional materials known as FA/Ni-MOF/5-FU.

The FT-IR confirms the structural stability of Ni-MOF across all samples. For Ni-MOF and Ni-MOF/5-FU, peaks include 3425 cm^{-1} (O–H stretching), 3219 cm^{-1} (aromatic C–H),[30] 2980 cm^{-1} (N–H), 1618 cm^{-1} (C═O from carboxylate), 1032 cm^{-1} (C–O).[31,32] The absence of ~1700–1730 cm^{-1} peaks indicate full ligand deprotonation. Identical spectra for Ni-MOF and Ni-MOF/5-FU suggest physical encapsulation of 5-FU within pores, with no significant chemical interaction or new peaks from 5-FU. In FA/Ni-MOF, peaks shift slightly: 3380 cm^{-1} (broadened O–H/N–H), 2889 cm^{-1} (enhanced N–H), 1670 cm^{-1} (C═O influenced by FA carbonyls), 1341 cm^{-1} (C–N), 1009 cm^{-1} (C–H/C–O related), and 583 cm^{-1} (O–Ni–O).[33] These changes confirm successful FA surface functionalization *via* coordination and hydrogen bonding, while preserving the MOF framework. The FA/Ni-MOF/5-FU composite retains FA-modified features with stable O–Ni–O, indicating intact structure, FA targeting moiety on the surface, and encapsulated 5-FU. This

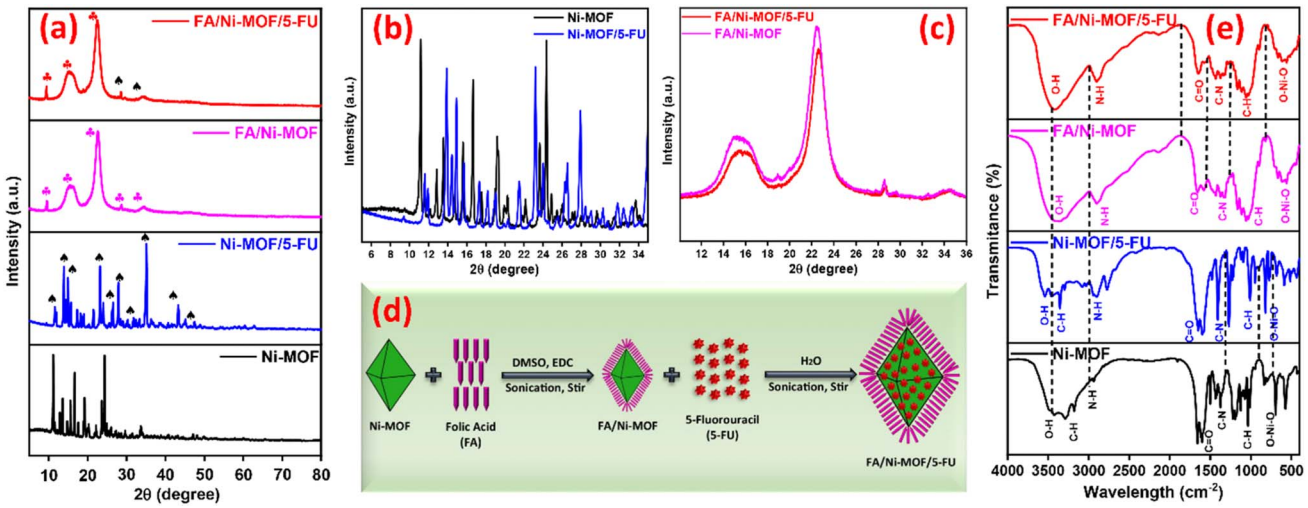

Fig. 1 (a) XRD of Ni-MOF, Ni-MOF/5-FU, FA/Ni-MOF and FA/Ni-MOF/5-FU (b and c) magnified version (d) reaction mechanism of the FA/Ni-MOF/5-FU (e) FTIR of Ni-MOF, Ni-MOF/5-FU, FA/Ni-MOF and FA/Ni-MOF/5-FU.

indicates formation of a stable, targeted drug delivery system with physical drug loading and effective FA conjugation.

The FA/Ni-MOF/5-FU composite exhibits a zeta potential of −25.37 mV (Fig. 2a) signifies good colloidal stability, as values beyond ±25 mV typically indicate sufficient electrostatic repulsion between particles. Conductivity (0.692 mS cm^{-1}) supports stable dispersion in the medium. The *Z*-average particle size of 162.6 nm (Fig. 2b) with a low polydispersity index (PDI = 0.2151), indicating a narrow and uniform particle size distribution. The Di (50) value of 179.5 nm confirms that most particles fall within the nanoscale range, while the Di (90) of 300.7 nm suggests the presence of a few larger aggregates.[34] These results demonstrate that FA and 5-FU incorporation into the Ni-MOF framework successfully produces stable, nanosized particles ideal for sustained and controlled drug delivery applications.

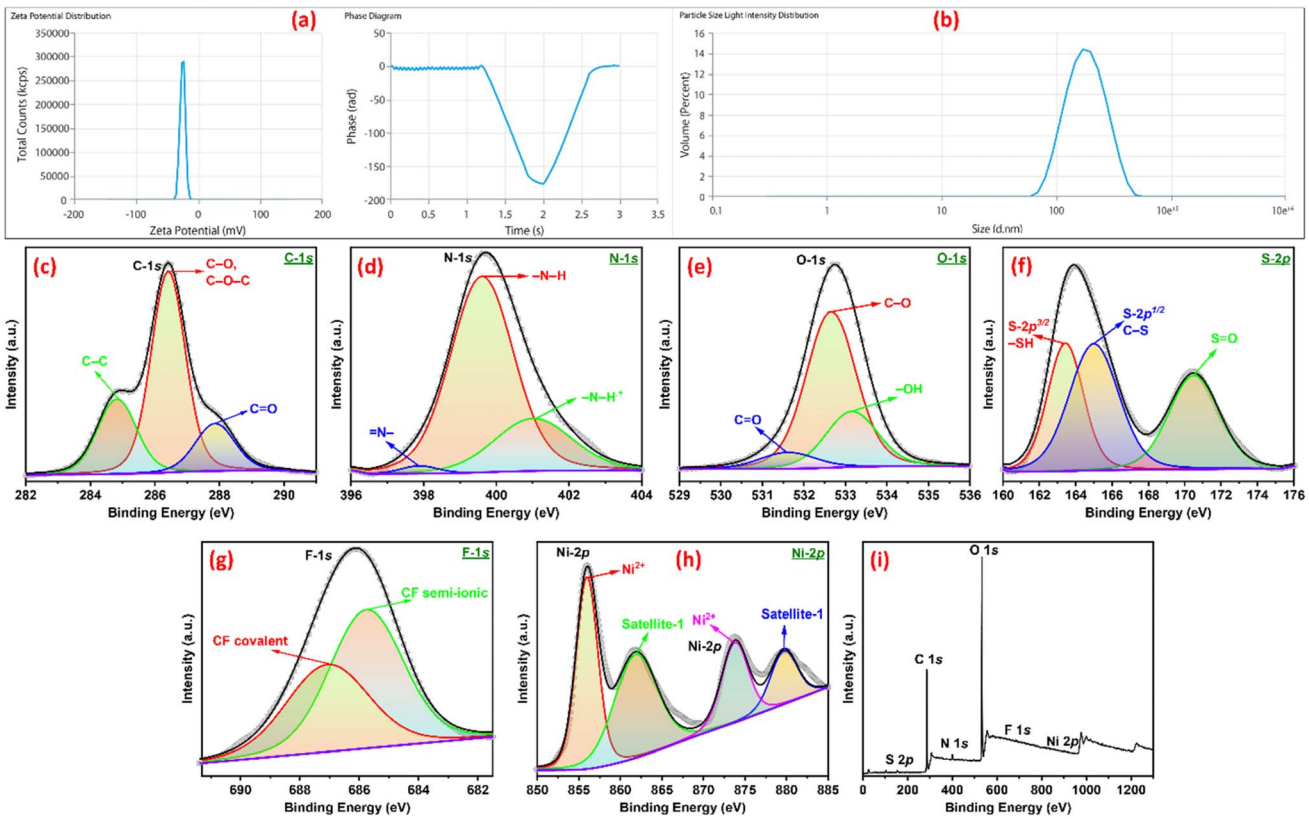

Fig. 2 (a) Zeta potential (b) DLS Z-average size, XPS spectra of (c) C (d) N (e) O (f) S (g) F (h) Ni and (i) survey of the FA/Ni-MOF/5-FU.

The signal of XPS spectra will commonly appear as atom-specific peaks, which can be deconvoluted in sub-peaks corresponding to the diverse atom-specific linkages involved in the chemical structure. Usually, the C-1s orbital is taken as the central peak and lignin polymers, located at the binding energy of 286.4 eV (Fig. 2c). The C-1s peak can be deconvoluted into several peaks corresponding to the main linkages of lignin and starch, such as C–C, C–O, O–C–O/C═O.[35] The region of interest of the deconvoluted peaks is positioned at 284.9–284.5, 286.4–286.0, and 287.8 eV, for C–C, O–C–O/C–O, C═O respectively. N-1s peak showed four components (Fig. 2d), while the weak intensity N 1s peak showed the presence of only three components (Fig. 2d). In line with the literature, the components at ~400 eV are assigned to neutral nitrogen in the MOF structure (–N–H structures), whereas the components shifted to the higher binding energies are most likely related to the positively charged nitrogen of polaron (–N–H^+) and bipolaron (═N–H^+) species. The component with the lowest binding energy, at 397.9 eV, corresponds to imine (═N–) structure.[36] The peaks of O-1s (531.6, 532.6, and 533.2 eV) shown in (Fig. 2e) can be attributed to the C═O, C–O, and –OH groups in lignin. In (Fig. 2f), the position of –SH was red-shifted after adsorption, which may be a piece of solid evidence for the involvement of –SH in the adsorption. Positions of S-$2p^{3/2}$ binding energy compared to the positions of S-2p, indicating that –SH. In addition, the peak near 170.5 eV indicates that sulfur oxides are also involved in the adsorption process.[37] The F-1s spectra were also obtained to confirm the presence fluorine of 5-FU (Fig. 2g). There were two fitted peaks: 685.6 and 686.9 eV for CF (semi-ionic and covalent) of 5-FU. As shown in (Fig. 2h), Ni^{2+} and Ni^{3+} were completely characterized *via* the Ni-2p emission spectrum, exhibiting two shake-up satellites. The fitting peaks at 855.9 eV and 874.1 eV correspond to Ni^{2+}, whereas the peaks at 862.1 eV and 879.7 eV are ascribed to Ni^{3+}.[38] Fig. 2i presents the XPS survey spectrum, showing the characteristic peaks for carbon (C), nitrogen (N), oxygen (O), nickel (Ni), fluorine (F) and sulfur (S), with distinct binding energies confirming the successful incorporation of each element into the FA/Ni-MOF/5-FU.

The HRTEM images (Fig. 3a–c) of the FA/Ni-MOF/5-FU composite reveal a well-defined nanostructured morphology with uniformly distributed particles, indicating a homogeneous framework. Fig. 3b displays clear lattice edges with a measured interplanar spacing of 0.368 nm, confirming the high crystallinity of the material and the preservation of the MOF structure after drug and ligand incorporation. SAED pattern (Fig. 3c) indicates that the composite has a polycrystalline structure and good order.

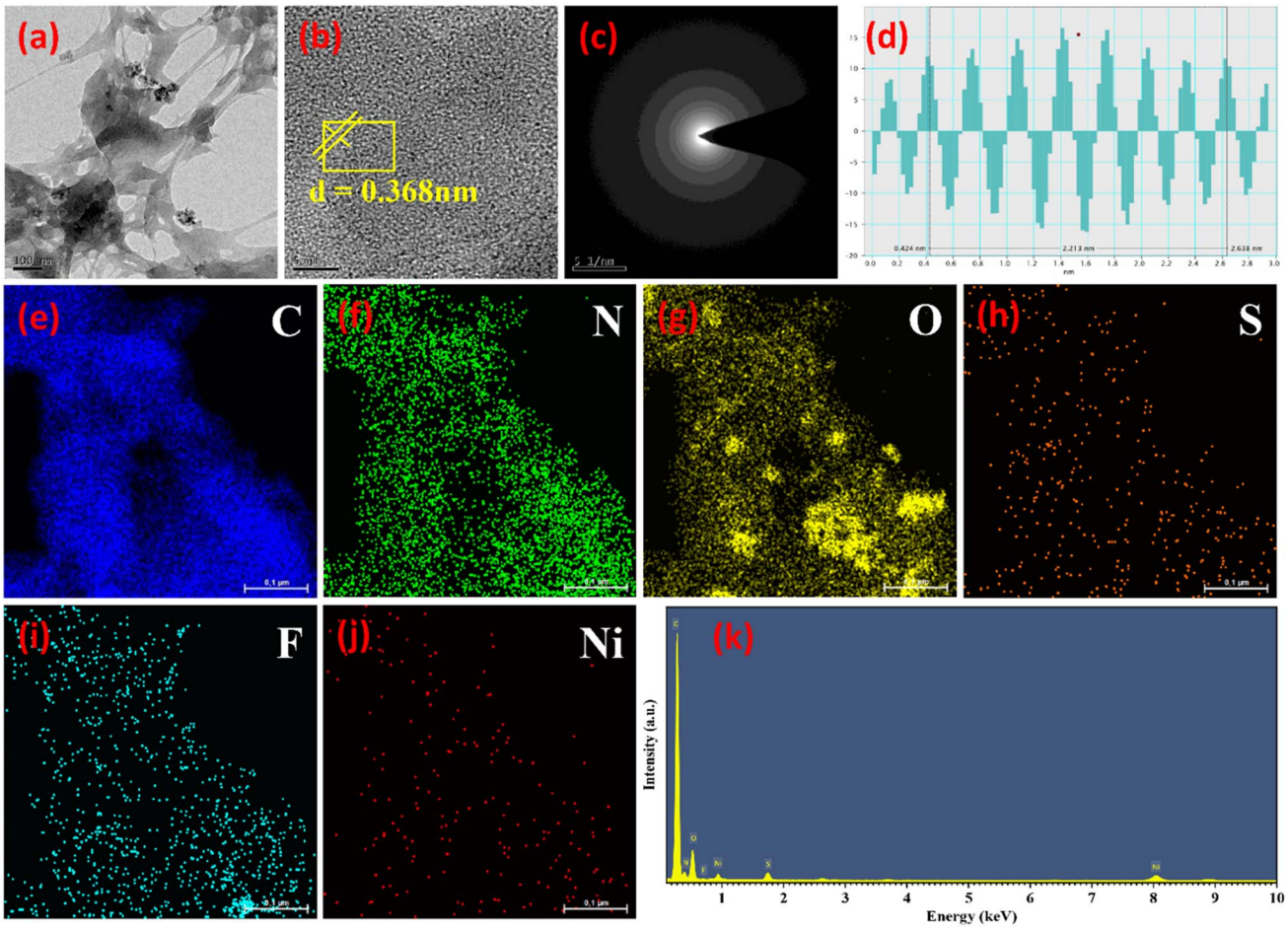

Fig. 3 HRTEM images of FA/Ni-MOF/5-FU (a) at 100 nm (b) at 5 nm and its *d*-spacing (c) SAED pattern at 5–1 nm (d) surface profile graph of FA/Ni-MOF/5-FU (e–j) elemental mapping of FA/Ni-MOF/5-FU (k) EDX spectra of FA/Ni-MOF/5-FU.

The lattice 'finger' images (Fig. 3d) have the same spacing as that of the crystalline framework seen using HRTEM. Element distribution images (Fig. 3e–j) indicate homogeneous element distribution throughout the whole structure, demonstrating that FA and 5-FU were successfully integrated into the Ni-MOF framework. The presence of C, N, O, S and Ni in the EDX spectrum (Fig. 3k) indicates that the FA/Ni-MOF/5-FU composite is made up of these elements. C, N, O and S represent the organic linkers with FA attached; F represents 5-FU encapsulated in the composite; and Ni represents the metal nodes of the MOF structure. Due to their good crystallinity, uniform distribution of elements, and strong structural integrity, the FA/Ni-MOF/5-FU nanocomposite can be considered an excellent candidate for stable and effective drug delivery systems.

Fig. 4a–d demonstrate the changes in morphology and drug content after incorporating 5-FU and FA into Ni-MOF. The pristine Ni-MOF (Fig. 4a) shows a crystalline structure, while 5-FU loading (Fig. 4b) introduces more porosity and increased density. The addition of FA (Fig. 4c) further enhances the surface density through interfacial bonding, creating a more porous structure in the FA/Ni-MOF/5-FU composite (Fig. 4d), which allows for better drug diffusion. The particle size

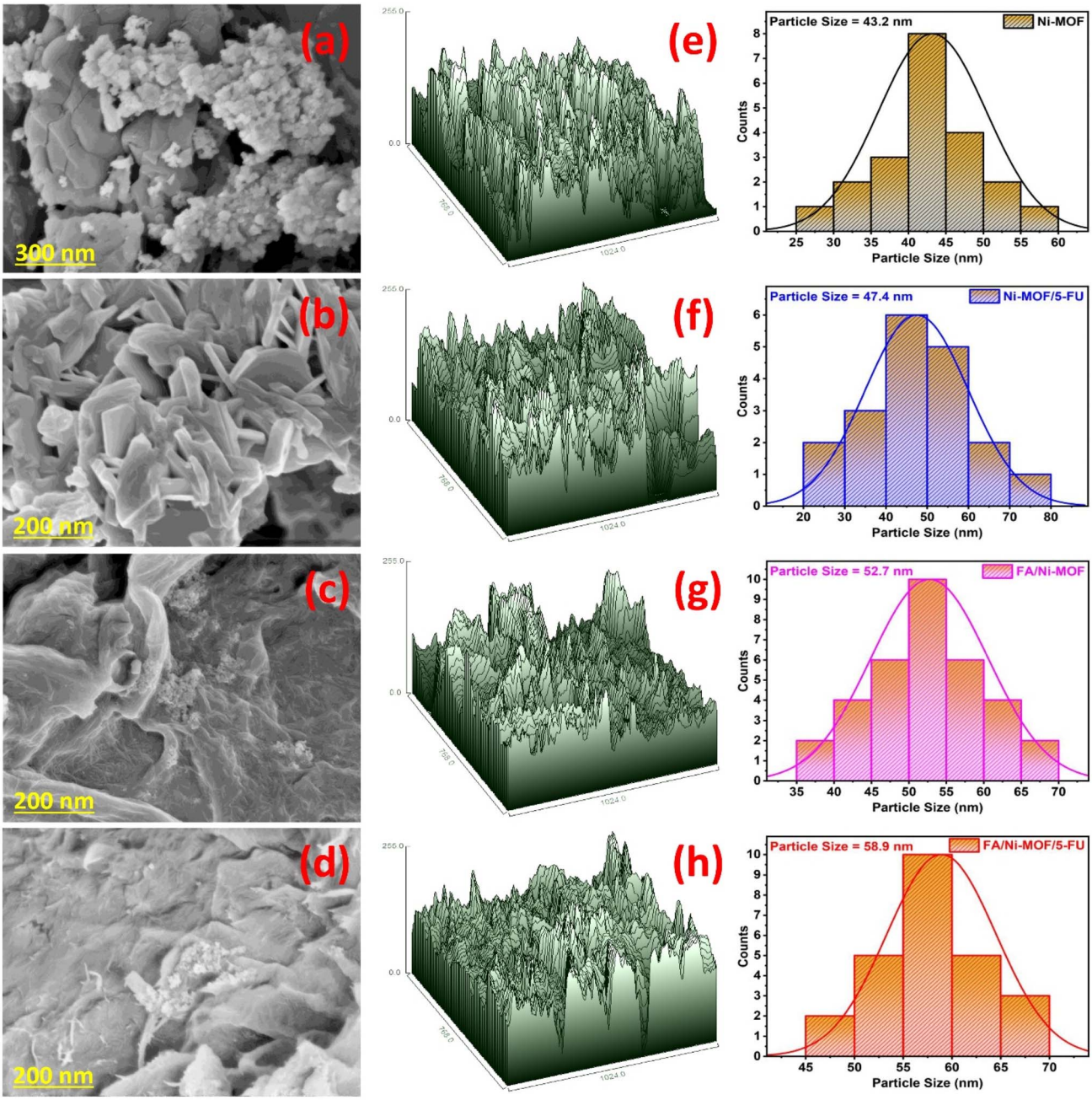

Fig. 4 SEM images of (a) Ni-MOF (b) Ni-MOF/5-FU (c) FA/Ni-MOF (d) FA/Ni-MOF/5-FU, histogram and surface plot of (e) Ni-MOF (f) Ni-MOF/5-FU (g) FA/Ni-MOF (h) FA/Ni-MOF/5-FU.

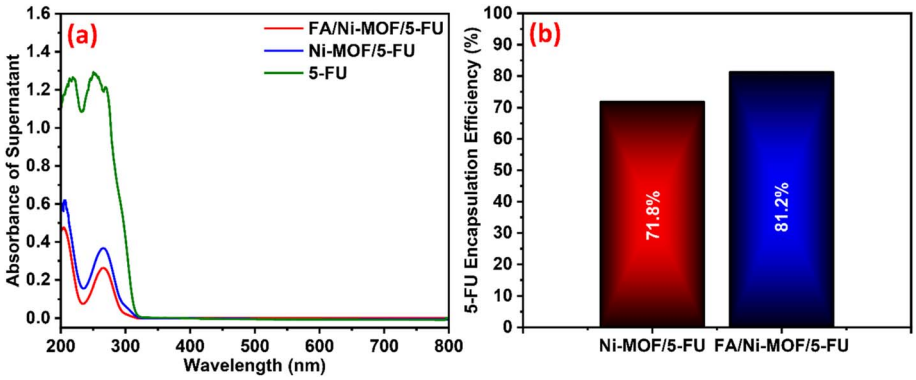

Fig. 5 (a) UV-Visible spectroscopy of 5-Fluorouracil (5-FU), Ni-MOF/5-FU, and FA/Ni-MOF/5-FU (b) encapsulation efficiency of Ni-MOF/5-FU and FA/Ni-MOF/5-FU.

distribution (Fig. 4e–h) reveals an increase in average particle size from 43.2 nm for Ni-MOF to 58.9 nm for FA/Ni-MOF/5-FU, indicating greater functionalization and drug loading. These structural changes improve the material's biocompatibility and promote sustained drug release, making Ni-MOF more effective for drug delivery.

3.1 Drug loading and drug release

UV-Visible (Fig. 5a) spectral analysis of FA/Ni-MOF/5-FU confirms that FA has been properly entrapped into the MOF matrix. The characteristic absorbance peaks of FA at the wavelengths between 260–270 nm were found to be less intense in the spectra of FA/Ni-MOF/5-FU relative to that of FA, that there are strong interactions between FA and the MOF material. The reduced sharpness of these absorbance peaks suggests that FA molecules are successfully encapsulated within the 3-dimensional Ni-MOF porous structure rather than remaining as free entities in solution. The differences in peak intensities and position are attributed to the presence of coordination bond formations between 5-FU molecules and the Ni^{2+} atom centers and 5-FU oxygen and nitrogen atoms, as well as hydrogen bonding and electrostatic attraction between FA and 5-FU due to the folic acid (–COOH, –OH) functional groups.[39] The presence of folic acid aids in providing additional interaction sites for stronger drug binding due to the larger number of bond formations and hydrogen bond interactions between FA and 5-FU molecules, leading to stabilized of the 5-FU molecule within the Ni-MOF porous material. The encapsulation efficiency (EE%) of FA/Ni-MOF/5-FU was 81.2% (Fig. 5b), which represents an increase in EE% compared to the Ni-MOF/5-FU composite (71.8%), further validating the synergistic benefits of folic acid aiding in drug loading enhancement due to the development of a robust Ni–O/N coordination network between 5-FU and the Ni^{2+} center and multiple hydrogen-bonded networks between FA and 5-FU molecules.[40] Due to its improved packaging stability and effectiveness, the FA/Ni-MOF/FU system is ideal for use as a continuous form of a drug delivery system with structural integrity, as well as for its biocompatible surface properties. Ni was chosen for its biocompatibility, stability, and ability to form pH-responsive, porous structures for controlled drug release. Folic acid functionalization minimizes nickel ion leakage, and stability studies in PBS (pH 7.4) showed that Ni-MOF remains intact.

Fig. 6a shows the pH-responsive drug release profile of FA/Ni-MOF/5-FU as well as the difference in release behaviour for acidic condition (pH = 5.0) and physiological (pH = 7.4) environments indicating the ability of FA/Ni-MOF/5-FU system to preferentially target tumors. FA/Ni-MOF/5-FU at pH = 5 (the simulated acidic environment of the tumor) has a much higher release (71.7%) over a period of time 180 h then FA/Ni-MOF/5-FU at pH = 7.4 (31%). In addition, the pH responsive release

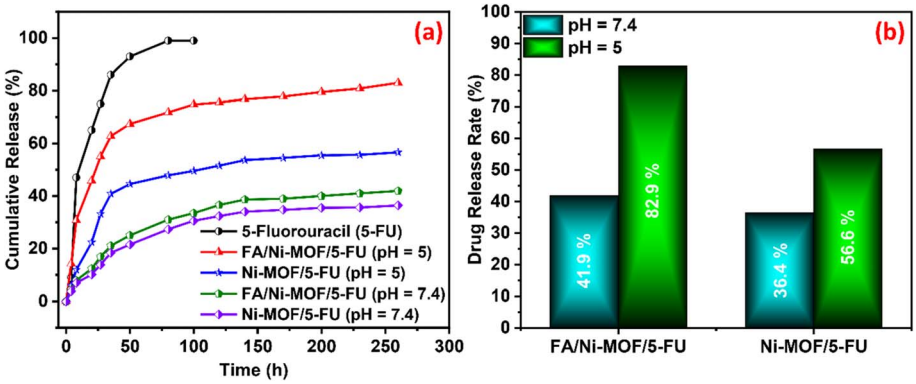

Fig. 6 (a) Cumulative release of 5-fluorouracil (5-FU), FA/Ni-MOF/5-FU & Ni-MOF/5-FU at pH 7.4 and 5 (b) percentage release of FA/Ni-MOF/5-FU, Ni-MOF/5-FU at pH 7.4 and 5.

behaviour of the FA/Ni-MOF/5-FU system is due to a combination of two mechanisms – (1) the complete/partial protonation of the folate group functional groups COOH and NH_2 in the folic acid and (2) the disruption of the co-ordination bond between Ni^{2+} and 5-FU due to an acid environment results in a controlled drug release.[41] Without the FA coating, the drug release from a Ni-MOF/5-FU is significantly lower at 47.8% and 27.3% at pH = 5.0 and pH = 7.4 respectively indicating that FA an important role in increasing the pH sensitivity/release efficiency. Fig. 6b demonstrates the influence of FA by functionalization has increased the release of FA/Ni-MOF/5-FU at pH = 5.0 while simultaneously protecting against uncontrolled premature leakage of drug from Ni-MOF(5-FU) at physiological pH (7.4). The findings support that FA/Ni-MOF/5-FU is an effective pH-sensitive and tumor-targeted delivery vehicle to deliver high therapeutic amounts of 5-FU at the cancer site while preventing instability and decreasing the side effects of 5-FU due to accumulation.

3.2 Mechanism of drug release

Scheme 6 depicts the FA/Ni-MOF/5-FU nanocarrier's mechanism for delivering drugs to specific cancer cells using folic acid (FA) as a targeting agent and responding to changes in pH. After being injected, the nanocarrier is taken up by the tumor cells *via* a receptor-mediated endocytosis process that relies on folate receptors (FR-α) that are at high levels on tumor types (breast tumor). Because the FR-α receptors are present in high concentrations on the surface of cancer cells and therefore bind to FA, exploited this interaction to improve the uptake and retention of the nanocarrier at the tumor site. Under physiological conditions (pH = 7.4), the Ni-MOF is stable because of the strong Ni–O coordination bonds, which prevents the premature leakage of drug (31%) after 180 hours. In the lower (more acidic) pH environment of the tumor (pH = 5.0), the carboxylate groups of the linkers become protonated, and the strength of Ni–O bonds are decreased, thus leading to the controlled breakdown of the MOF structure and the subsequent controlled release of 5-fluorouracil (5-FU) from the nanocarrier. 5-FU is then able to diffuse into the cytoplasm and nucleus of the tumor cells, where it disrupts DNA and RNA synthesis and ultimately cause the cancer cells to undergo apoptosis. The combination of FA-mediated active targeting and pH-sensitive release of the drug contribute to the nanocarrier's high therapeutic efficiency and reduced "off-target" toxicity and preferential drug accumulation within the tumor tissue, establishing the FA/Ni-MOF/5-FU nanocarrier as a novel, effective, and good platform for targeted cancer therapy.[42]

3.3 *In Vitro* cytotoxicity study

The anticancer efficacy and biocompatibility of free 5-fluorouracil (5-FU), Ni-MOF, Ni-MOF/5-FU and FA/Ni-MOF/5-FU were evaluated using the MTT assay against MDA-MB-231 human breast cancer cells and MCF-10A normal breast epithelial cells after 24 hours of incubation at 37 °C in a 5% CO_2 atmosphere (Fig. 7). As presented in Table 1, the free 5-FU drug exhibited substantial cytotoxicity toward MDA-MB-231 cells, achieving 71.23% inhibition at 40 μM (IC_{50} = 24.4 ± 0.6 μM), but it also showed significant toxicity toward normal MCF-10A cells, with

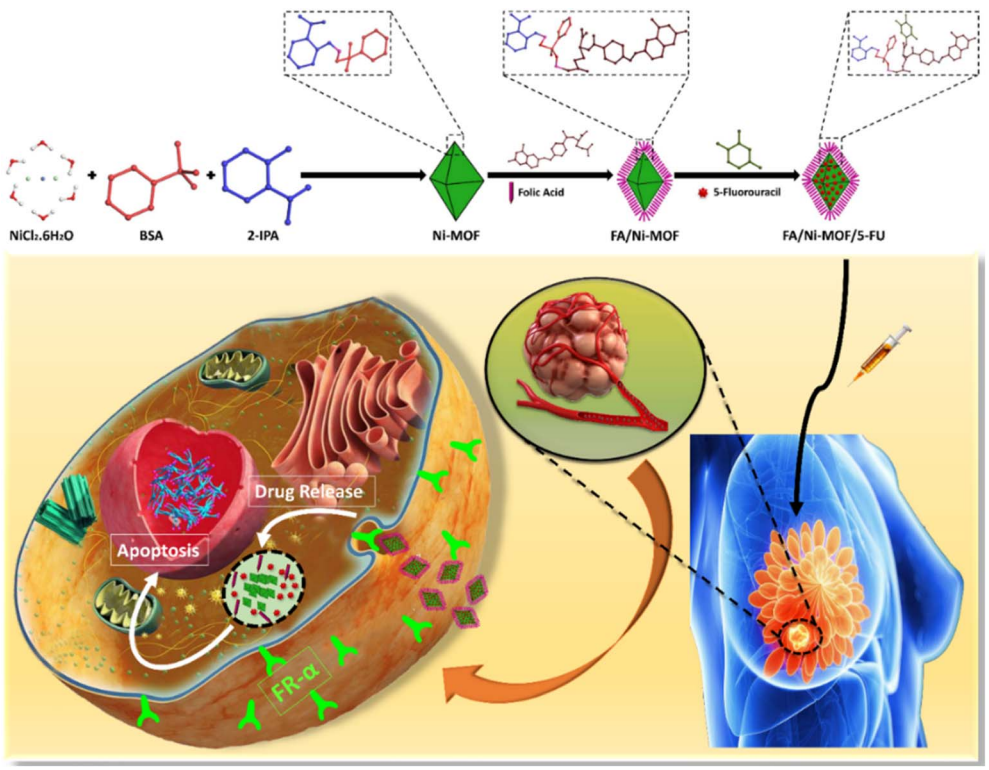

Scheme 6 Mechanism scheme for the targeted drug delivery.

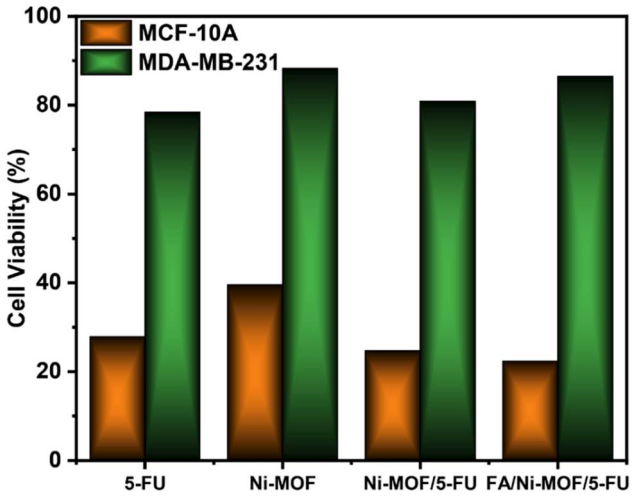

Fig. 7 *In vitro* cell viability of MDA-MB-231 (breast cancer cells) and MCF-10A cells after 24 h incubation at 37 °C in 5% CO_2 with 5-fluorouracil (5-FU), FA/Ni-MOF/5-FU, Ni-MOF/5-FU and Ni-MOF at a concentration of 40 μM.

78.43% viability inhibition (IC_{50} > 40 μM), indicating a lack of tumor selectivity. FA/Ni-MOF/5-FU nanocomposite shows the highest anticancer activity, reaching 83.51% inhibition against MDA-MB-231 cells (IC_{50} = 18.5 ± 0.4 μM), while maintaining 86.54% viability in MCF-10A cells (only 16.34% inhibition, IC_{50} > 40 μM). This difference demonstrates that folic acid functionalization enhances the targeted uptake of the nanocarrier through folate receptor (FR-α)-mediated endocytosis, which is overexpressed on breast cancer cells, resulting in higher intracellular accumulation and enhanced cytotoxicity in tumor tissue while sparing normal cells.[43] Ni-MOF exhibited moderate anticancer activity (58.91% inhibition, IC_{50} = 37.8 ± 0.5 μM) and high cell viability in normal cells (88.32%), confirming its biocompatibility and intrinsic structural safety. The progressive enhancement in cytotoxic performance from Ni-MOF → 5-FU → FA/Ni-MOF/5-FU highlights the synergistic effect of drug encapsulation and FA surface modification, which improve cellular selectivity, sustained drug release, and reduced off-target toxicity. The lower IC_{50} for FA/Ni-MOF/5-FU in cancer cells indicates higher cytotoxicity specifically toward tumor cells, not normal cells, due to the targeted delivery *via* folate receptor-mediated endocytosis. In normal cells, FA/Ni-MOF/5-FU shows much less toxicity, which demonstrates improved selectivity and reduced systemic toxicity. The IC_{50} values for normal cells (MCF-10A) remain high, supporting the claim of enhanced biocompatibility and tumor-selective cytotoxicity. The dose response behavior and IC_{50} values convincingly establish FA/Ni-MOF/5-FU as a promising tumor-specific and

Table 1 Cytotoxicity results of MDA-MB-231 (breast cancer cell) and MCF-10A cell line at 40 μM

		MDA-MB-231			MCF-10A		
Compounds	Conc (μM)	% Cell viability	% Inhibition	IC_{50} values	% Cell viability	% Inhibition	IC_{50} values
Normal (control)	—	100	0	—	100	0	—
5-Fluorouracil 5-FU (standard)	40	27.89^{***}	71.23^{***}	24.4 ± 0.6	78.43^{*}	22.42^{*}	>40
FA/Ni-MOF/5-FU	40	22.37^{***}	83.51^{***}	18.5 ± 0.4	86.54^{*}	16.34^{*}	>40
Ni-MOF/5-FU	40	24.71^{***}	75.32^{***}	23.6 ± 0.4	80.88^{*}	17.54^{*}	>40
Ni-MOF	40	39.53^{***}	58.91^{***}	37.8 ± 0.5	88.32^{*}	13.63^{*}	>40

The data is indicated as % viability and % inhibition at 40 μM for each compound. $n = 3$, one way ANOVA, compared to normal control group ($^{*}p < 0.05$, $^{***}p < 0.001$). The respective IC_{50} values for each compound in both cell lines are given.

Table 2 Comparison table of previous literature

Sr	Compounds	Drug loading Capacity (%)	Stimulus	Drug release (%)	Time (h)	Cancer Cells	Cancer type	Ref.
1	Fe_3O_4@MOF-DOX-CDs-Apt	62	pH	47.3	96	MDA-MB-231	Breast cancer	44
2	ZIF-8@LTZ@CS-FA	85.5 ± 2.3	pH	75	120	MCF-7	Breast cancer	45
3	FA-NH_2-UiO-66@5-FU	30.26 wt%	pH	62	48	HeLa cells	Cervical cancer	46
4	Co-MOF@5-FU	27 ± 3 wt%	pH	75	120	EOMA hemangioma cells	Vascular tumor	47
5	5-FU@FeMn-MIL-88B	43.8 wt%	pH	70	24	HEK293T	Human embryonic kidney cells	48
6	5-FU@MOF-808-15%/PDA	56.82	pH	60.2	24	MCF-7	Breast cancer	49
7	5-FU@CS/Zn-MOF@GO	45	pH	41.5	72	MDA-MB-231	Breast cancer	50
8	FC-(Ni/Ta) MOF-DOX	81	pH	51	72	MCF-7	Breast cancer	51
9	5-FU@(FeCo)bi-MIL-88B-FC	29.8	pH	58	48	SW480	Colon cancer	52
10	FA/Ni-MOF/5-FU	81.2	pH	71.7	80	MDA-MB-231	Breast cancer	This Work

safer nanocarrier system for targeted breast cancer therapy. The IC_{50} > 40 μM for free 5-FU in normal cells, coupled with 78.43% viability, indicates that while 5-FU exhibits significant cytotoxicity in cancer cells, the drug is less selective for normal cells. At higher concentrations, the normal cells show some resistance mechanisms, preventing complete cell death. The importance of highlighted targeted delivery systems like FA/Ni-MOF/5-FU, which improves drug selectivity and minimizes off-target effects. Also literature are added into the Table 2.

Both % inhibition and IC_{50} values were calculated from the same dose–response curve generated using the MTT cytotoxicity assay. The inhibition percentages were determined at different concentrations, and the IC_{50} was derived by fitting the dose–response data to a nonlinear regression model to determine the concentration at which 50% of cell viability was inhibited.

The FA/Ni-MOF/5-FU nanocarrier exhibited enhanced selectivity toward MDA-MB-231 breast cancer cells compared with normal MCF-10A breast epithelial cells. This selectivity can be attributed to folate receptor–mediated uptake and the biocompatible Ni-MOF core, which provides a stable, porous structure for drug loading and controlled release. FA functionalization improves targeting, while the Ni-MOF's porous structure ensures efficient drug delivery to cancer cells. The MTT cytotoxicity assay further confirmed the selective cytotoxicity, indicating that the Ni-MOF platform not only supports stability and targeted drug delivery but also contributes to reduced systemic toxicity and improved biosafety of the nanocarrier system.

4 Conclusion

The FA/Ni-MOF/5-FU nanoplatform demonstrated remarkable potential in enhancing 5-fluorouracil delivery for targeted breast cancer therapy. The incorporation of folic acid (FA) modification with nickel-based metal–organic frameworks (Ni-MOF) enabled efficient folate receptor-mediated targeting of MDA-MB-231 breast cancer cells, leading to significantly improved anticancer efficacy. Cytotoxicity assays revealed that FA/Ni-MOF/5-FU achieved 83.51% inhibition in MDA-MB-231 cells at 40 μM (IC_{50} = 18.5 ± 0.4 μM), outperforming free 5-fluorouracil (71.23% inhibition, IC_{50} = 24.4 ± 0.6 μM) and unmodified Ni-MOF/5-FU (75.32% inhibition, IC_{50} = 23.6 ± 0.4 μM). FA/Ni-MOF/5-FU nanoplatform exhibited enhanced biocompatibility, showing high viability in normal MCF-10A breast epithelial cells (86.54% viability, IC_{50} = 16.34 μM) compared to free 5-FU (78.43% viability, IC_{50} = 22.42 μM). The uncoated Ni-MOF displayed minimal cytotoxicity toward both cancer and normal cells, confirming it's better for health. These findings underscore the superior tumor selectivity, pH-responsive release behavior, and reduced systemic toxicity of the FA/Ni-MOF/5-FU nanoplatform, positioning it as a promising and safer alternative to conventional 5-fluorouracil chemotherapy for breast cancer treatment. This study highlights an innovative folic acid-mediated nanocarrier system that offers a more effective and targeted approach for overcoming the limitations of traditional chemotherapy, way for improved therapeutic precision and patient outcomes.

Author contributions

Komal Zaman Khan, Ammar Saleem, Ali Junaid: investigation, methodology, writing – original draft. Aurang Zaib, Ghazanfar Abbas, Zahid Shafiq: investigation, formal analysis, software. Eman Fayad, Dalal Nasser Binjawhar: investigation, validation, funding acquisition, resources. Muhammad Naeem Ashiq, Hua Li Qin: conceptualization, supervision, writing – review & editing.

Conflicts of interest

The authors declare no conflicts of interest.

Data availability

The data supporting this article have been included as part of the supplementary information (SI). Supplementary information is available. See DOI: https://doi.org/10.1039/d6ra00551a.

Acknowledgements

We are grateful to Wuhan University of Technology for Support. The authors extend their appreciation to Princess Nourah bint Abdulrahman University Research Supporting Project number (PNURSP2026R155), Princess Nourah bint Abdulrahman University, Riyadh, Saudi Arabia.

References

1 Y. Zhang, Y. Ji, S. Liu, J. Li, J. Wu, Q. Jin, X. Liu, H. Duan, Z. Feng and Y. Liu, Global burden of female breast cancer: new estimates in 2022, temporal trend and future projections up to 2050 based on the latest release from GLOBOCAN, *J. Natl. Cancer Cent.*, 2025, **5**, 287.
2 E. Nivethaa, J. Sivasankari, S. Baskar, C. A. Martin and N. Kalkura, Folic acid conjugated magnetic chitosan nanocomposite for the targeted delivery of dual anticancer drugs to breast cancer and hyperthermia therapy, *Int. J. Biol. Macromol.*, 2025, 147303.
3 D. Su, Y. Cui, C. He, P. Yin, R. Bai, J. Zhu, J. S. Lam, J. Zhang, R. Yan and X. Zheng, Projections for prevalence of Parkinson's disease and its driving factors in 195 countries and territories to 2050: modelling study of Global Burden of Disease Study 2021, *BMJ*, 2025, **388**, e080952.
4 N. Kokila, B. Mahesh, K. Roopa, B. D. Prasad, K. Raj, S. Manjula, K. Mruthunjaya and R. Ramu, Thunbergia mysorensis mediated nano silver oxide for enhanced antibacterial, antioxidant, anticancer potential and in vitro hemolysis evaluation, *J. Mol. Struct.*, 2022, **1255**, 132455.
5 D. K. Sharma and R. Saripilli, Recent strategies in diagnosis, screening, prevention, and treatment of breast cancer in young women, *Discov. Oncol.*, 2025, **16**, 1532.
6 A. Zafar, S. Khatoon, M. J. Khan, J. Abu and A. Naeem, Advancements and limitations in traditional anti-cancer therapies: a comprehensive review of surgery,

chemotherapy, radiation therapy, and hormonal therapy, *Discov. Oncol.*, 2025, **16**, 607.

7 A. Mishra, V. L. Gole and S. Ojha, Smart nanocarriers in triple-negative breast cancer: recent advances in targeting and translational application, *Drug Deliv. Transl. Res.*, 2025, 1–25.

8 I. D. A. Wilujeng, A. P. Pramono, Y. S. Tjang and R. Puspita, Therapeutic evaluation of bone marrow mesenchymal stem cells for hepatitis virus infection: immunoregulation, anti-inflammatory effects, and clinical potential-a systematic review, *Mol. Biol. Rep.*, 2025, **52**, 819.

9 B. Roopashree, B. Mahesh, R. Ramu, N. Rekha, S. Manjula, G. Preethi and V. Gayathri, An insight into the cytotoxic, antimicrobial, antioxidant, and biocontrol perspective of novel Iron (III) complexes of substituted benzimidazoles: Inhibition kinetics and molecular simulations, *J. Biomol. Struct. Dyn.*, 2024, **42**, 11538–11554.

10 P. Tarighi, S. M. M. Esfahani, A. Emamjomeh, S. Z. Mirjalili and P. Mirzabeigi, Optimizing cancer treatment: A comprehensive review of active and passive drug delivery strategies, *Iran. Biomed. J.*, 2025, **29**, 173.

11 A. K. Srivastav, P. K. Rajput, J. Jaiswal, U. C. Yadav and U. Kumar, In vitro and in silico investigation of glycyrrhizic acid encapsulated zein nanoparticles: a synergistic targeted drug delivery approach for breast cancer, *Int. J. Biol. Macromol.*, 2024, **266**, 131368.

12 R. Perveen, S. Bibi, M. A. Saleem, M. H. Helal, A. Afzal, M. A. Wattoo and A. ur Rehman, Recent progress in ZIF–polymer composites for advanced drug delivery applications, *J. Mater. Chem. B*, 2025, **13**, 6949–6989.

13 A. Magadla, Hybrid Nanoplatforms Based on Photosensitizers and Metal/Covalent Organic Frameworks for Improved Cancer Synergistic Treatment Nano-Delivery Systems, *Molecules*, 2025, **30**, 884.

14 J. Swain, A. Priyadarshini, S. Panda, S. Hajra, N. Das, V. Vivekananthan, K. Mistewicz, R. Samantray, H. Joon Kim and R. Sahu, Metal–Organic Frameworks: Synthesis Methods and Multifunctional Applications, *Energy Technol.*, 2025, **13**, 2402354.

15 K. T. K. Reddy and A. S. Reddy, Recent breakthroughs in drug delivery systems for targeted cancer therapy: an overview, Cellular, *Cell. Mol. Biomed. Rep.*, 2025, **5**, 13–27.

16 C. Zhong, S. Wang, W.-J. Jiang, Z. Li, X. Wang, S. Fan, J. Huang, H.-J. Wu, R. Sheng and T. Fei, Chemoresistance mechanisms to 5-Fluorouracil and reversal strategies in lung and breast cancer, *Sci. Rep.*, 2025, **15**, 6074.

17 Z. Yang, C. L. Cespedes-Acuña, Z. Yang, M. Z. Abu Bakar, K. W. Chan and X. Deng, Plant foods and their bioactives as dietary enhancers for colon cancer treatment with 5-fluorouracil, *Food Rev. Int.*, 2025, **41**, 1390–1439.

18 A. Purohit, P. Nema and P. K. Panda, *Implications of Silica-Based Nanoparticles for Cancer Therapy, Metallic Nanoparticles in Cancer Therapy*, CRC Press, pp. , pp. 194–219.

19 A. Abed, M. Karimi, M. Nejati, M. R. Hamblin, S. A. Mirzaei, M. Sarvizadeh and H. Mirzaei, Synthesis of 5-Fluorouracil (5-FU) coated platinum nanoparticles and apoptotic effects on U87 human glioblastoma cells, *Cancer Cell Int.*, 2025, **25**, 280.

20 Y. An, C. Ji, H. Zhang, Q. Jiang, M. F. Maitz, J. Pan, R. Luo and Y. Wang, Engineered cell membrane coating technologies for biomedical applications: from nanoscale to macroscale, *ACS Nano*, 2025, **19**, 11517–11546.

21 A. K. Bakshi, T. Haider, D. Panwar, M. Sharma, P. Tiwari, N. Rai and V. Soni, Ligand density vs mechanistic insight: a ligand conjugated formulation for the treatment of triple-negative breast cancer, *J. Nanopart. Res.*, 2025, **27**, 248.

22 M. Beiranvand and G. Dehghan, An analytical review of the therapeutic application of recent trends in MIL-based delivery systems in cancer therapy, *Microchim. Acta*, 2025, **192**, 89.

23 P. Raju, K. Balakrishnan, M. Mishra, T. Ramasamy and S. Natarajan, Fabrication of pH responsive FU@ Eu-MOF nanoscale metal organic frameworks for lung cancer therapy, *J. Drug Delivery Sci. Technol.*, 2022, **70**, 103223.

24 J.-J. Shen, S.-J. Xue, Z.-H. Mei, T.-T. Li, H.-F. Li, X.-F. Zhuang and L.-M. Pan, Synthesis, characterization, and efficacy evaluation of a PH-responsive Fe-MOF@ GO composite drug delivery system for the treating colorectal cancer, *Heliyon*, 2024, **10**, e28066.

25 F. Yang, Q. Dong, Z. Chen, B. Gao, D. Zheng, R. Wang, S. Qin, F. Peng, M. Luo and J. Yang, A ph-responsive drug-delivery system based on apatinib-loaded metal-organic frameworks for ferroptosis-targeted synergistic anti-tumor therapy, *Int. J. Nanomed.*, 2024, 9055–9070.

26 A. Ahmed, A. Karami, R. Sabouni, G. A. Husseini and V. Paul, pH and ultrasound dual-responsive drug delivery system based on PEG–folate-functionalized Iron-based metal–organic framework for targeted doxorubicin delivery, *Colloids Surf., A*, 2021, **626**, 127062.

27 A. Kazemi, M. H. Afshari, H. Baesmat, S. Keshavarz, F. Zeinali, S. Zahiri, E. Torabi, F. Manteghi and S. Rohani, Room-temperature synthesis of pH-responsive MOF nanocarriers for targeted drug delivery in cancer therapy, *J. Polym. Environ.*, 2025, 1–12.

28 F. Kalantarnia, S. Maleki, A. Shamloo, K. Akbarnataj and S. N. Tavoosi, A thermo-responsive chitosan-based injectable hydrogel for delivery of curcumin-loaded polycaprolactone microspheres to articular cartilage: In-vitro and in-vivo assessments, *Carbohydr. Polym. Technol. Appl.*, 2025, **9**, 100678.

29 A. H. Betseba and Y. C. Shaji, Surface Area Enhanced Synthesis of Cu and Ni-based Metal-Organic Frameworks for Photocatalytic Degradation of Malachite Green Dye and Anticancer Drug Delivery Applications, *J. Drug Delivery Sci. Technol.*, 2025, 107138.

30 S. Sahoo, C. Chakraborti and S. Mishra, *FTIR and Raman Spectroscopic Investigations of Controlled Release Ofloxacin/HPMC Mucoadhesive Suspension*, 2011.

31 J. Zhuang, M. Li, Y. Pu, A. J. Ragauskas and C. G. Yoo, Observation of potential contaminants in processed biomass using fourier transform infrared spectroscopy, *Appl. Sci.*, 2020, **10**, 4345.

32 N. Thakur and N. Thakur, *Examining the Photocatalytic and Antioxidant Properties of Tripled Doped Co-ni-zn TiO2 Nanoparticles: A New Class of Nanocatalyst Synthesized by Chemically and Biologically Approach Using Microwave-Assisted Method*, 2024.

33 A. I. Stepanov, V. S. Sannikov, D. V. Dashko, A. G. Roslyakov, A. A. Astrat'ev and E. V. Stepanova, A rational method of synthesis and chemical properties of 5-(4-aminofurazan-3-yl)-1-hydroxytetrazole, *Chem. Heterocycl. Compd.*, 2017, **53**, 746–759.

34 R. Raychaudhuri, A. Pandey, A. Hegde, S. M. Abdul Fayaz, D. K. Chellappan, K. Dua and S. Mutalik, Factors affecting the morphology of some organic and inorganic nanostructures for drug delivery: characterization, modifications, and toxicological perspectives, *Expet Opin. Drug Deliv.*, 2020, **17**, 1737–1765.

35 Z. Rashedi, *A Study in Lignin Capability to Improve Strength and Water Absorbency of Starch Polymers: a Potential Heat-Resistant Fluid-Loss-Controller in Water Based Drilling Fluids*, 2021.

36 N. Luhakhra and S. K. Tiwari, Polaron and bipolaron mediated photocatalytic activity of polypyrrole nanoparticles under visible light, *Colloids Surf., A*, 2023, **667**, 131380.

37 S. Hou, S. He, T. Zhu, J. Li, L. Ma, H. Du, W. Shen, F. Kang and Z.-H. Huang, Environment-friendly preparation of exfoliated graphite and functional graphite sheets, *J. Materiomics*, 2021, **7**, 136–145.

38 Z. Fu, J. Hu, W. Hu, S. Yang and Y. Luo, Quantitative analysis of Ni2+/Ni3+ in Li [NixMnyCoz] O2 cathode materials: Non-linear least-squares fitting of XPS spectra, *Appl. Surf. Sci.*, 2018, **441**, 1048–1056.

39 B. Liu, Y. Chen, J.-L. He, J. Wu and W.-M. Sun, Computational Screening of Metal-Doped Borospherene B40 for 5-Fluorouracil Drug Delivery, *Comput. Theor. Chem.*, 2025, **1253**, 115443.

40 M. Fischer, *Adsorption of the Anticancer Drug 5-fluorouracil in Faujasite-type Zeolites Studied with Density Functional Theory Calculations*, 2024.

41 A. D. O. Adeyemo, *Modulation of Apoptosis and its Regulatory Proteins in Colorectal Cancer Cells: Effect of Oxidant Quenching and NSAIDs on (5 FU) Chemotherapy-Induced Toxicity*, University of London, University College, London (United Kingdom, 2003.

42 D. Fan, Y. Cao, M. Cao, Y. Wang, Y. Cao and T. Gong, Nanomedicine in cancer therapy, *Signal Transduct. Targeted Ther.*, 2023, **8**, 293.

43 A. Narmani, M. Rezvani, B. Farhood, P. Darkhor, J. Mohammadnejad, B. Amini, S. Refahi and N. Abdi Goushbolagh, Folic acid functionalized nanoparticles as pharmaceutical carriers in drug delivery systems, *Drug Dev. Res.*, 2019, **80**, 404–424.

44 H. Alijani, A. Noori, N. Faridi, S. Z. Bathaie and M. F. Mousavi, Aptamer-functionalized Fe3O4@ MOF nanocarrier for targeted drug delivery and fluorescence imaging of the triple-negative MDA-MB-231 breast cancer cells, *J. Solid State Chem.*, 2020, **292**, 121680.

45 M. Ghaderpour, S. Kashanian, M. Nazari, M. Motiei and S. Sajadimajd, Targeted delivery of letrozole using a modified metal–organic framework as a promising candidate in breast cancer therapy, *BioNanoScience*, 2024, **14**, 2872–2885.

46 H. Dong, G. X. Yang, X. Zhang, X. B. Meng, J. L. Sheng, X. J. Sun, Y. J. Feng and F. M. Zhang, Folic acid functionalized zirconium-based metal–organic frameworks as drug carriers for active tumor-targeted drug delivery, *Chem.–Eur. J.*, 2018, **24**, 17148–17154.

47 Q.-Q. Wang, Z.-P. Yang, Z.-T. Cui, X.-H. Wang and Y. Lin, A microporous Co (II)-MOF as a pH-responsive 5-Fu delivery system to induce human hemangioma cells apoptosis and abrogate their growth, *J. Coord. Chem.*, 2020, **73**, 1436–1449.

48 M. U. Akbar, M. Badar and M. Zaheer, Programmable drug release from a dual-stimuli responsive magnetic metal–organic framework, *ACS Omega*, 2022, **7**, 32588–32598.

49 A. Kazemi, H. Aghamirza Moghim Aliabadi, M. H. Afshari, M. Tamtaji, H. Baesmat, S. Keshavarz, F. Zeinali, E. Torabi, G. S. Ferdowsi and F. Manteghi, Porosity Modification in MOF Nanocarriers for pH-Responsive Drug Delivery in Cancer Therapy, *ACS Appl. Bio Mater.*, 2025, **8**, 7830–7841.

50 M. Pooresmaeil, E. A. Asl and H. Namazi, A new pH-sensitive CS/Zn-MOF@ GO ternary hybrid compound as a biofriendly and implantable platform for prolonged 5-Fluorouracil delivery to human breast cancer cells, *J. Alloys Compd.*, 2021, **885**, 160992.

51 S.-s. Jalaladdiny, A. Badoei-dalfard, Z. Karami and G. Sargazi, Co-delivery of doxorubicin and curcumin to breast cancer cells by a targeted delivery system based on Ni/Ta core-shell metal-organic framework coated with folic acid-activated chitosan nanoparticles, *J. Iran. Chem. Soc.*, 2022, **19**, 4287–4298.

52 M. U. Akbar, S. Khattak, M. I. Khan, U. A. K. Saddozai, N. Ali, A. F. AlAsmari, M. Zaheer and M. Badar, A pH-responsive bi-MIL-88B MOF coated with folic acid-conjugated chitosan as a promising nanocarrier for targeted drug delivery of 5-Fluorouracil, *Front. Pharmacol*, 2023, **14**, 1265440.